The Flying Monkey: a Mesoscale Robot that can Run, Fly, and Grasp

Yash Mulgaonkar[1], Brandon Araki[3], Je-sung Koh[2], Luis Guerrero-Bonilla[1], Daniel M. Aukes[2], Anurag Makineni[1], Michael T. Tolley[4], Daniela Rus[3], Robert J. Wood[2], and Vijay Kumar[1]

***Abstract*— The agility and ease of control make a quadrotor aircraft an attractive platform for studying swarm behavior, modeling, and control. The energetics of sustained flight for small aircraft, however, limit typical applications to only a few minutes. Adding payloads – and the mechanisms used to manipulate them – reduces this flight time even further. In this paper we present the flying monkey, a novel robot platform having three main capabilities: walking, grasping, and flight. This new robotic platform merges one of the world's smallest quadrotor aircraft with a lightweight, single-degree-of-freedom walking mechanism and an SMA-actuated gripper to enable all three functions in a 30 g package. The main goal and key contribution of this paper is to design and prototype the flying monkey that has increased mission life and capabilities through the combination of the functionalities of legged and aerial robots.**

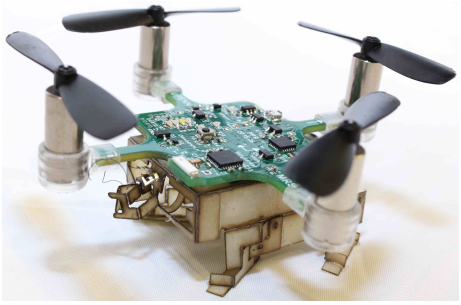

Fig. 1: Our 30g flying monkey. Videos of the experiments conducted are available as a video attachment and at `http://mrsl.grasp.upenn.edu/yashm/ICRA2016.mov`.

I. INTRODUCTION

Recent trends in robotics showcase the possibilities of novel manufacturing techniques, ever-shrinking electronic systems, and new concepts in swarm behavior. High-power motor/driver systems, small-form-factor lithium batteries, and compact board designs have produced systems composed of tens of quadrotor aircraft capable of stable, controlled swarming flight [1] [2]. Low-cost, single board designs have permitted simple robotic systems to be scaled to thousand-robot swarms [3]. Related manufacturing techniques inspired by origami and popup books have allowed small, electromechanical systems to be tightly integrated into flying and walking systems at a variety of size scales, while providing several possible methods for scaling mechanism assembly to a high number of devices [4]–[6].

Despite their many technical innovations, micro- and mesoscale robots face a common set of problems. Since they are made in small batches, they must be built by hand, so manufacturing steps such as board population, device interconnection, and mechanical assembly are laborious affairs. In addition, their small size corresponds to small battery capacities, so these robots can last for less than an hour on the ground and minutes in the air. Furthermore, small robots are typically single-function, making their use cases extremely limited; they are suitable as toys and educational platforms, but not for general robotics applications.

We hypothesize that combining multiple capabilities in the same device will make robots more robust and allow them to overcome the challenges of reduced battery life and limited use cases. Walking, compared to flying, is a relatively safe, low-power state where the impact of a failing battery has fewer unfavorable effects and the cost of not moving is closer to zero. Walking potentially permits the device to carry heavier payloads and access vertically-limited spaces where flying is not safe or possible. Adding flying to a walking-only machine permits the device to travel quickly and escape from difficult terrain. The option of both modes of locomotion allows the device to optimize over either speed or energy consumption. The combination of both capabilities also enables hybrid control scenarios where steering can be provided by propellers, resulting in a simpler, lighter walking mechanism.

Similarly, the ability to grasp objects in combination with multi-modal locomotion permits a device to transport objects, reconfigure its surroundings, and interact with other devices. In this paper, we present a centimeter-scale robot capable of more than just terrestrial locomotion, flight, or grasping. By combining these three functions, we hope to develop a new class of robots capable of not just operating in the world, but of accessing it more completely, interacting with it, and modifying it.

II. BACKGROUND

The mobility and efficiency of a mobile robot can be greatly improved by combining two modes of locomotion.

[1]Y. Mulgaonkar, L. Guerrero-Bonilla, A. Makineni and V. Kumar are with the GRASP Laboratory, University of Pennsylvania, Philadelphia, PA 19104, USA. {yashm, luisg, makineni, kumar}@grasp.upenn.edu

[2]J.-S. Koh, D. Aukes, and R. J. Wood are with Harvard University and the Wyss Institute for Biologically Inspired Engineering.

[3]B. Araki and D. Rus are with CSAIL, The Stata Center, Building 32 32 Vassar Street Cambridge, MA 02139 USA

[4]M. T. Tolley is with the Department of Mechanical and Aerospace Engineering, University of California, San Diego.

Fig. 2: A sequence of photographs demonstrating the multi-modal trajectory tracking capability of the flying monkey.

When flying is involved, researchers have striven to minimize additional mass in their implementations of multi-modal locomotion in order to reduce energy consumption. For example, by morphing wings into legs, a flying robot can walk without the need for additional leg mechanisms, thereby reducing complexity and the overall weight of the robot [7]. Alternatively, by adding a simple and light rolling cage, a quadrotor can sustain flight after collisions and also roll along the floor to save energy with terrestrial locomotion [8]. However, there are still many unexplored ways to achieve multi-modal locomotion with simple and lightweight structures. Origami-inspired laminate devices show promise for testing new designs and mechanisms thanks to their potential for rapid prototyping and fast design iteration.

A. Folded Laminate Devices

Origami-inspired designs and mechanisms facilitate rapid prototyping of robotic systems, saving time and effort. Popup book MEMS processes [4] with smart composite structures [9] and PopupCAD [10] have enabled us to construct a crawler that has a lightweight and simple folding mechanism using sheet materials and an origami-inspired design. There are currently many examples of folded laminate devices that have proven that they can replace conventional mechanical systems with simple folding structures with functions of sensing and monitoring, gripping [11], locomotion [12], mobile manipulation [11], and self-folding for the assembly of structures [13], [14] and robots [15].

B. Multi-modal Locomotion

Nature has many examples of animals such as bats and flying insects that use multiple modes of locomotion to navigate highly variable environments and, presumably, to optimize between speed and energy efficiency. The benefits of multi-modal locomotion have been demonstrated by various robots. R. Bachmann et al. [16] combined a fixed-wing micro air vehicle (MAV) with a crawling robot. The resulting 30.5cm robot had a cruising air speed of 11 m/s compared to a maximum ground speed of 0.33 m/s; however, it had a flight time of 15 minutes versus a maximum crawling time of 100 minutes, demonstrating the potential of flight for fast, high-power locomotion and crawling for slow, high-efficiency locomotion. Jumping and gliding robots have also been shown to increase mobility and efficiency. The MultiMo-Bat in M. Woodward et al. [17] jumps 3m vertically and glides 2.3m horizontally with 115.6g in body mass and 30cm in the largest dimension of the robot. A. L. Desbiens et al. [18] show another jump gliding robot that has a pivoting wing that reduces the drag in jumping mode. This jump gliding robot achieved a greater range of motion and lower cost of transport than a ballistic jumping robot.

III. FOLDED LAMINATE CRAWLER

A. Kinematics of the Crawler's Leg Mechanism

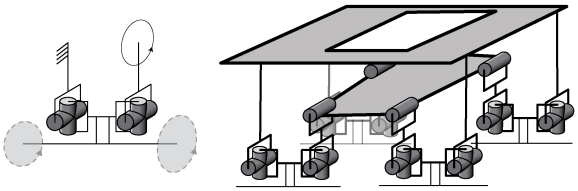

(a) (b)

Fig. 3: Kinematics of the single leg mechanism consists of two universal joints (a), and a mechanism that has four hips and eight feet (b).

The crawling mechanism is based off of the hexapod DASH mechanism developed at UC Berkeley [19]. However, our design has eight feet; four outer feet and four inner feet that contact the ground alternately. The symmetry of the eight-legged mechanism allows four feet to bear the weight of the robot equally at all times. In a hexapod design, one foot on one side of the robot bears twice the weight of two feet on the other side of the robot. Due to the compliance of the joints, the symmetric eight-legged mechanism was preferable to a hexapod mechanism because it minimized asymmetries in the deformation of the legs and feet.

The kinematics are shown in Fig. 3. A motor mounted to the frame of the robot is used to rotate the central shaft, which in turn moves the four hips. Each hip has two feet, one pointing in and one pointing out. Both feet follow a circular trajectory but are 180 degrees out of phase, so that the outer foot touches the ground when the inner foot is in the air and vice-versa.

A series four-bar mechanism was added to the crawler in order to constrain the degrees of freedom of the leg mechanism to the y- and z- directions. The crawler has only one degree of freedom so that it can move only forward and backward. Steering is achieved by taking advantage of the yaw torque of the integrated quadrotor and compliance in the joints of the crawler.

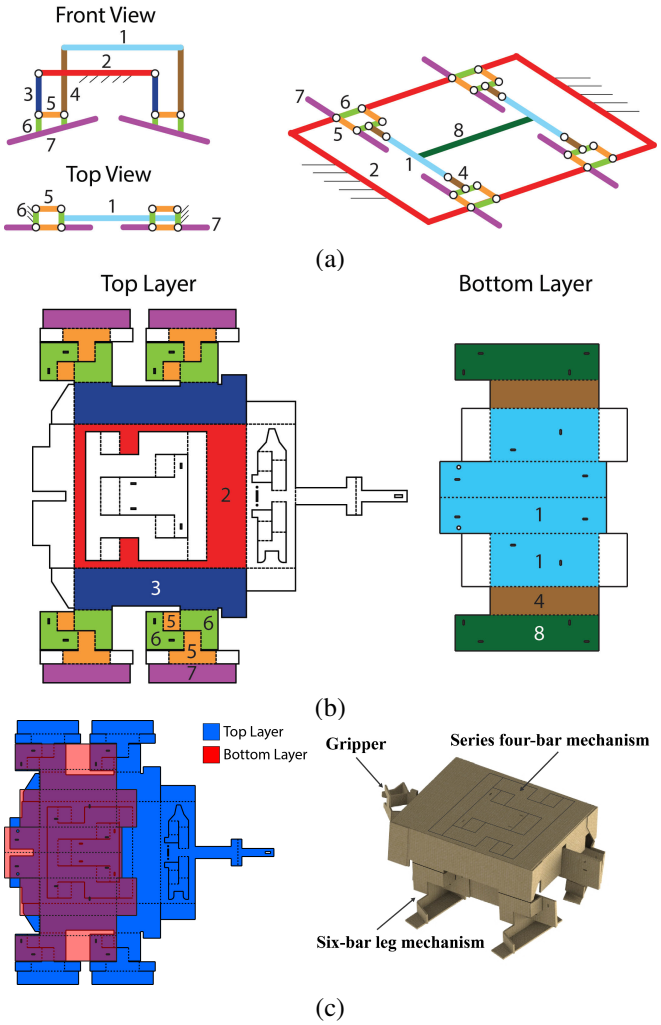

Fig. 4: Pattern design of the crawler (a, b) Color-coded diagrams of the kinematic structure of the robot correspond to linkages in the 2-D layout of the top and bottom laminates (c) The bottom laminate is overlaid on the top laminate and the structure is folded into a robot.

B. Laminate Pattern Design

The first step in designing the foldable crawler was to convert the kinematics of Fig. 3 into a linkage structure that consisted of rigid links and revolute joints as shown in Fig. 4(a). The linkage structure could then be translated directly into the fold patterns of Fig. 4(b). Links become faces and revolute joints become hinges, and each link in Fig. 4(a) corresponds to a face in Fig. 4(b) with the same color. The design was split into two sublaminates; the sublaminate on the right in Fig. 4(b) is glued onto the hips of the other sublaminate and serves as the central shaft that links the hips together. An illustration of the series four-bar mechanism that constrains the central shaft to rotate about a single axis can be seen in Fig. 5(b).

The gripper consists of two four-bar mechanisms with extensions that can be pulled together and pushed apart. The linkage structure and fold pattern of the gripper is illustrated

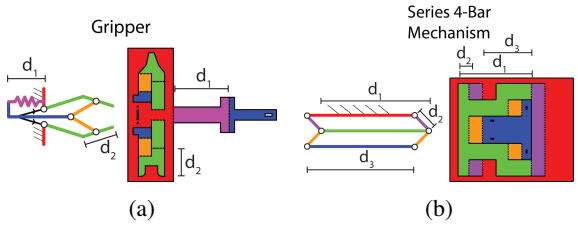

Fig. 5: Gripper and Series Four-Bar Mechanisms.

in Fig. 5(a). A built-in passive spring pulls the gripper in so that the gripper is closed by default. A shape memory alloy (SMA) coil is used to pull the main shaft of the gripper out to open it. Fig. 6 shows a closeup of the gripper in its open (Fig. 6b) and closed (Fig. 6a) positions. On the flying monkey, the onboard micro-controller controls the SMA actuator through one of the digital outputs and a high power MOSFET. Section IV describes the rest of the hardware of the flying monkey in detail.

The maximum gripping load was measured by testing what weights the gripper could support before grasp failure. Weights were suspended from a segment of a drinking straw, and the gripper was clamped around the straw. The weights started at 1.4g, then 2g, then increased in 1g increments until the straw slipped from the gripper. A test was considered a failure if the straw slipped out of the gripper and a success if it did not. The results are shown in Fig 6. The value of the maximum gripping load can be increased by a surface treatment for a high friction coefficient.

C. Fabrication

Recent advances in techniques for analyzing laminate geometries, determining manufacturability, and automating the creation of laminate device manufacturing files have yielded positive results for quickly generating articulated, multi-material electromechanical devices [6]. These devices, though designed and manufactured in-plane, are capable of complex three-dimensional motion and can be linked together to form even-higher-dimensional motion with some guarantees that they can be manufactured using simple, planar, manufacturing processes and straight-line out-of-plane assembly and removal motions [20]. These components can be saved and reused in an object-oriented fashion using a purpose-built software tool called popupCAD [21], a design suite that stores and operates upon layered sets of planar geometries.

The walking mechanism was designed and fabricated using this laminate design process. Sketches were created that designated the placement of three basic design components: rigid body material, flexible hinge locations, and gap geometries that separate rigid bodies. The rigid body sketches consisted of polygons and other filled shapes. The hinge sketches consisted of one or more line segments that allowed the placement and reuse of hinge geometry used to connected rigid bodies together. popupCAD was then used to generate a set of manufacturable cut files that allowed the design to be cut and laminated from sheets of flat material. FR4, an

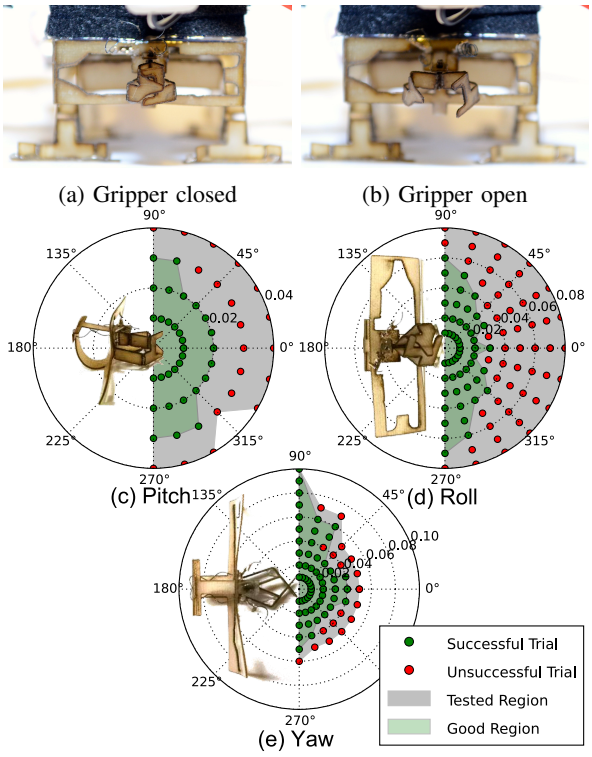

Fig. 6: The gripper mechanism(a,b), Gripper pull-out force data in (c) pitch, (d) roll and (e) yaw. Radial axes are displayed in 0.02ND segments, and rotational segments are in 15-degree increments. Trials with successful grasps are shown in green, and failures in red.

epoxy/fiberglass laminate, was used for the rigid layers; 1 mil PET was used for the flexible layer; and heat activated mounting adhesive film was used for the adhesive layers. The cut sheets were laminated together and cut once more to create an interconnected set of rigid elements separated by flexible hinges. Hot glue or super glue was then used to glue the two sublaminate layers together; hot glue was also used to secure tabs that were built in to the design to provide structural support to the crawler.

IV. Dragonfly Quadrotor

The Dragonfly is the second generation of the pico quadrotor family [22]. Each 22g robot is constructed from a 0.047" thick double layer fiber-glass PCB. These robots are capable of extremely fast and agile flight reaching speeds of up to 6m/s and coming to a full stop, all within a 4m $\times$ 4m flight space. A modular design approach was employed for rapidly prototyping the circuit boards by creating an expansive design library of subsystem modules [23]. This facilitates rapid iterations in the PCB design, limiting the schematic redesign to mere high-level interconnects with the central processor and other subsystems.

A. Autopilot

In order to build the smallest and lightest autonomous quadrotor, we designed the autopilot from the ground-up.

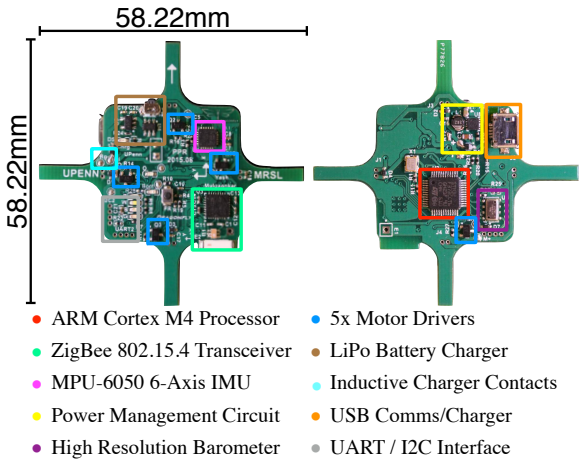

Fig. 7: Components of the Dragonfly quadrotor autopilot.

Realizing the true potential of quadrotor MAVs, a wide variety of autopilots are now commercially available. Among the multitude of options, even the most widely used autopilots like the PX4 Pixhawk [24] though feature-rich, are rather bulky, weighing close to 36g, with a footprint averaging about 40cm^2. In contrast, our custom designed autopilot, shown in Fig. 7 spans a mere 3cm^2 and weighs only 4.8g without any compromise on features [22]. The Dragonfly is equipped with an ARM Cortex M4 STM32F373 microprocessor serving as the brain, which interfaces with Atmel's AT86RF212 900MHz 802.15.4 wireless transceiver chip. An InvenSense MPU-6050 6-axis MEMS gyroscope & accelerometer and a Measurement Specialties MS5611 high precision barometer allow for accurate attitude and altitude measurement, while a 3.3V Buck/Boost switching regulator powers all the subsystems while maintaining a consistent logic level throughout the circuit. Five 4A DC brushed motor drivers power the motors and an integrated Lithium Polymer $(LiPo)$ battery charging circuit allows for in-system charging of the on-board battery. A micro USB port and two multipurpose I2C and UART ports allow for interfacing with a wide range of external sensors.

This 0.047" thick, double layered autopilot also serves as the main structural component of the Dragonfly, eliminating the need for an additional load bearing frame. 3D printed snap-on motor mounts are used to attach the motors to the autopilot. Finally, a single cell 3.7V, 240mAh Li-Po battery powers the Dragonfly, giving it a six minute flight time.

V. Flying Monkey

The primary goal of this paper was to explore the design, characterization and fabrication of a small scale multi-modal robot capable of fast, agile flight and crawl into tight, confined spaces, for reconnaissance or search and rescue (SaR) type situations.

A. Characterization

The remainder of this section provides an insight into the effect of scaling on vehicle mass. Following our previous analysis of the pico quadrotor [22], the predecessor to the

Dragonfly, we divide the total mass of the flying monkey into six categories — Battery, Motors & Propellers, Frame, Crawler, Electronics, and Miscellaneous (adhesives, fasteners etc.)

Fig. 8 shows the mass distribution of various components of the flying monkey. We see that the origami inspired crawler contributes about 17% to the total mass of the robot. The battery and propulsion system are the heaviest components, comprising 27% and 33%, attesting to the fact that LiPo batteries and DC brushed motors scale poorly with reduction in size. The printed circuit board, also serving as the frame of the robot, contributes about 13%, while the electronics contribute a modest 7% of the total mass of the robot.

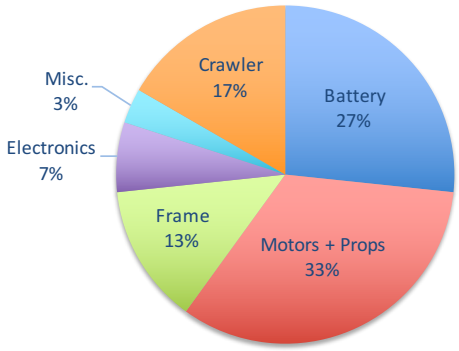

Fig. 8: Mass Distribution of the flying monkey (m = 0.03kg).

B. Mathematical model and control

We use a simple model to study the behavior of the flying monkey while crawling:

$$\begin{bmatrix} \dot{x}(t) \\ \dot{y}(t) \\ \dot{\theta}(t) \end{bmatrix} = \begin{bmatrix} v(t)cos(\theta(t)) \\ v(t)sin(\theta(t)) \\ u(t) \end{bmatrix} \tag{1}$$

where $x(t)$ and $y(t)$ are the cartesian position of the robot in the plane, $\theta(t)$ is the yaw angle, and $v(t)$ and $u(t)$ are the control inputs for the linear velocity and yaw velocity respectively. Let us define $e_\theta = \theta - \theta_d$, where θ_d is the desired yaw angle, and assume that $|e_{\theta max}| \leq \pi$. The control law for the yaw angle is selected as follows

$$u = -k_\theta \sin(e_\theta) + \dot{\theta}_d \tag{2}$$

where k_θ is a positive constant. For the linear velocity control law we use a controller similar to [25]. Let $\mathbf{x}$ be the position vector in the plane and $\mathbf{x}_d$ the desired position vector. Defining $\mathbf{e}_x = \mathbf{x} - \mathbf{x}_d$, the control law for the linear velocity is selected as follows:

$$v = \left[-k_x(\mathbf{e}_x) + \dot{\mathbf{x}}_d\right]^T \begin{bmatrix} \cos(\theta) \\ \sin(\theta) \end{bmatrix} \tag{3}$$

where k_x is a positive constant. Substituting eqns. 2 and 3 into eqn.1, it can be shown that

$$\dot{\mathbf{x}} = -k_x(\mathbf{e}_x) + \dot{\mathbf{x}}_d + \|-k_x(\mathbf{e}_x) + \dot{\mathbf{x}}_d\| \sin(e_\theta) | \tag{4}$$

$$\dot{\theta} = -k_\theta \sin(e_\theta) + \dot{\theta}_d \tag{5}$$

Substituting eqn.(2) into eqn. (1) and rearranging terms, we arrived to

$$\dot{e}_\theta = k_\theta \sin(e_\theta) = 0 \tag{6}$$

Within $|e_\theta| \leq \pi$, the yaw angle has only one stable equilibrium point at $|\theta - \theta_d| = 0$ so that e_θ converges asymptotically to 0 in this region. Consider now the Lyapunov function candidate

$$V = \frac{1}{2}\mathbf{e}_x^T\mathbf{e}_x + \frac{1}{2}e_\theta^2 \tag{7}$$

It can be shown that its time derivative is negative definite as long as

$$k_x k_\theta > \frac{\|\dot{\mathbf{x}}_d\|_{max}^2}{4\left(1 - |\sin(e_{\theta_{max}})|\right)} \tag{8}$$

where $\|\dot{\mathbf{x}}_d\|_{max}$ is the maximum value of the norm of $\dot{\mathbf{x}}_d$.

While this last constraint on the product of the gains k_x and k_θ might seem discouraging, it is important to notice that, since e_θ converges asymptotically to 0 independent of the position error $\mathbf{e}_x$, there is no need to use high gains if we allow some time for the robot to get to the right orientation.

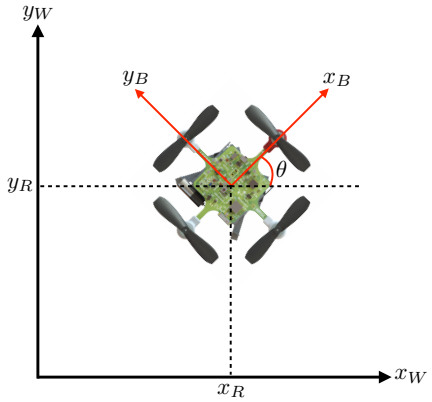

Fig. 9: Flying monkey coordinate system.

VI. Software Architecture

The mission planner for the robot is written in C++ using the ROS [26] (Robot Operating System) framework. The incorporation of ROS greatly simplifies the transition between computation on the base station and onboard the robot.

As seen in the architecture diagram in Fig. 10, a high level mission planner running on the base station reads in user input in the form of waypoints or time parametrized trajectories. The trajectory generator then sends calculated desired position commands to a state machine which analyzes the position commands and governs the mode of locomotion of

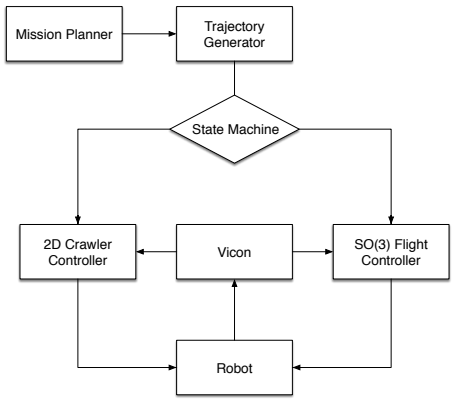

Fig. 10: Software Architecture for controlling the flying monkey.

the robot, delegating the control to either the 2D crawler controller for terrestrial, planar locomotion, or to the SO(3) flight controller for the current phase of the mission.

The integration of the finite state machine into ROS and C++ allows us to run closed loop controllers by using pose and position estimates from the Vicon motion capture system and the attitude state estimation on-board the MAVs.

The selected controller receives the robot's current pose and position from the motion capture system and the desired position from the trajectory generator. Using this information, the controller computes a desired attitude and thrust setpoint and transmits them to the robot through a 900MHz wireless uplink at a 100Hz. With these desired attitude and thrust measurements and its own onboard pose estimates, the robot computes and executes the appropriate motor commands to attain the desired setpoints. This low-level control loop onboard the robot, runs at the rate of 1kHz.

VII. ENERGETICS

Multi-modal robots like the flying monkey, that can crawl, grasp and fly, have tremendous potential in missions involving navigation in highly complex and constrained environments owing to their ability to crawl under or fly over obstacles. A wide range of use cases have sought small autonomous fliers. An inherent limitation of any such robot is the limited battery life, which dramatically affects effective mission life, maneuverability, and onboard functionality (e.g. sensing, computation). Given the ability of crawling, the flying monkey shows immense potential in addressing the issue of limited flight time of small aerial robots, with the added dexterity of ground based platforms. This section highlights the energetics of the two locomotion modalities of the flying monkey individually and as a union.

A. Energetics at hover

To obtain the energetics of the flying monkey, we measured the battery voltage of the robot using an onboard battery monitor and designed a custom power board consisting of a MAX4172 Current-Sense Amplifier to measure in-flight current draw. Fig. 11 shows the power draw of the standalone Dragonfly quadrotor and the flying monkey at hover. We empirically determined the power draw of the Dragonfly and the flying monkey to be 9.75W and 10.59W respectively.

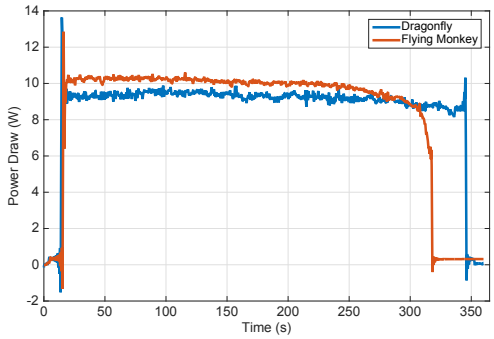

Fig. 11: Hover Power draw of the Dragonfly quadrotor P_{avg} = 9.75W and the flying monkey P_{avg} = 10.59W.

B. Energetics during crawling

Next, to determine the energetics during terrestrial locomotion, we recorded the voltage and current drawn by the flying monkey while crawling at its maximum speed of 0.16 m/s on a flat surface. We found that the power drawn while crawling was 0.64W – over 93% lower than the power consumption during flight. This is shown in Fig. 12. The figure shows a 45 minute data log, over which the battery voltage only dropped by a few millivolts, confirming the lower power draw for a ground robot.

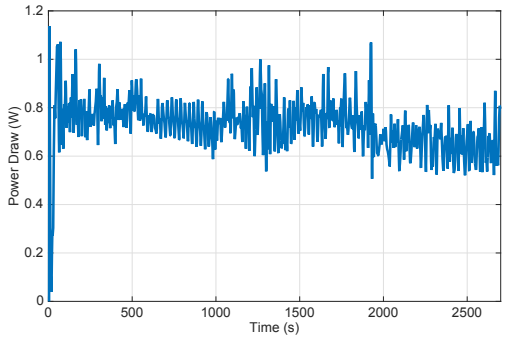

Fig. 12: Power draw of the flying monkey at 0.1m/s . P_{avg} = 0.64 W.

C. Cost of transportation

Next, to calculate the *Cost of transportation* (COT), we assumed that for all practical purposes, the power consumed P by the flying monkey while flying at a velocity v of 1m/s was equal to the power drawn at hover. Therefore, the cost of transportation for the flying monkey with a mass m = 0.03kg to cover a distance d of 1m, while flying at 1m/s and crawling at 0.16m/s, the cost of transportation is given by:

$$COT_f = \frac{P_f}{mgv_f} = \frac{10.59}{mg} = 35.99 \quad (9)$$

$$COT_c = \frac{P_c}{mgv_c} = \frac{0.64}{mg \cdot 0.16} = 13.67 \quad (10)$$

where, COT_f and COT_c are the cost of transportation for flying and crawling respectively.

This analysis builds a strong case for ground robots, showing that a purely aerial robot has a significantly higher cost of transportation compared to a ground robot. However, with some compromise and by combining the two locomotion modalities, the flying monkey can harness the potential of aerial locomotion while keeping the COT low.

VIII. Experimental Data

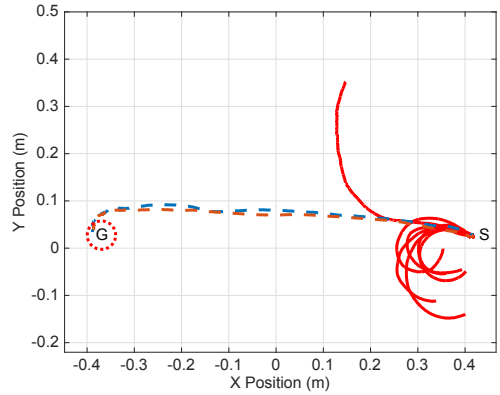

Fig. 13: Crawler performance with and without active controller.

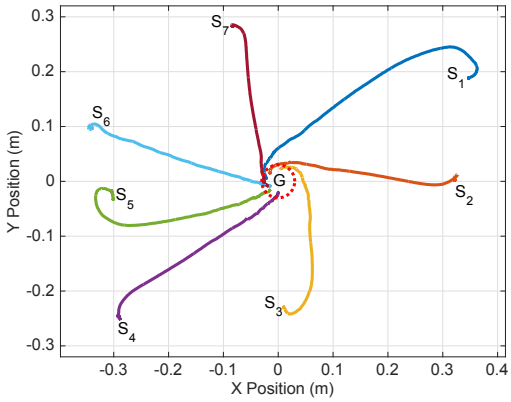

Fig. 14: Position regulation starting from different initial positions ($S_1 - S_7$) and orientations to the goal G.

A. Regulation and Time Parametrized Trajectory Tracking

Fig. 13 shows the performance of the robot at different speeds while trying to crawl from an initial position to a fixed destination: the solid lines in red show its performance without a controller, while the dotted lines show its performance using the controller described earlier. Fig. 14 shows the performance of the robot under feedback control crawling to a constant position from different initial positions and orientations. Fig. 15 shows the crawling performance of the robot tracking a reference moving in a circular trajectory of radius $8cm$ centered at the origin at approximately $-0.21rad/s$ while Fig. 16 shows the performance tracking the Lissajous curve described by $x(t) = 0.2cos(-0.01t)$, $y(t) = 0.2sin(-0.02t)$.

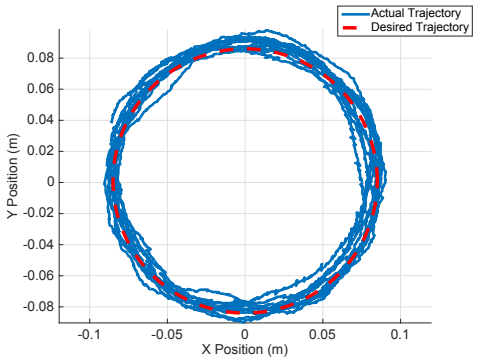

Fig. 15: Trajectory tracking performance along a circle.

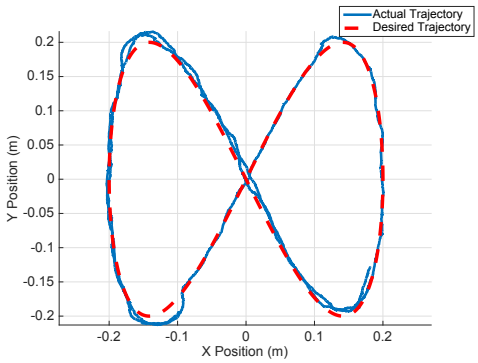

Fig. 16: Trajectory tracking performance along a Lissajous curve.

IX. Capabilities

Combining crawling, flying, and grasping into a single small and maneuverable package extends the capabilities of the flying monkey to execute complex tasks. For example, the flying monkey can optimize for speed and energy efficiency, flying to travel quickly and crawling to conserve energy. The flying monkey can hop over obstacles (as demonstrated in Fig. 2), and crawl under or through small openings, such as under a door or through a pipe. The gripper, in combination with these modes of locomotion, can be put to use in a number of situations. The flying monkey can easily pick up small objects (on the order of 6mm and 1-2g), although a larger and stronger gripper should enable it to pick up even larger objects. With its multi-modal capabilities, the flying monkey can pick up an object while in crawler mode, deliver it to its destination by air, and then return to crawler mode to deposit the object. These capabilities make the flying monkey a powerful tool for object retrieval/delivery and, when coordinated in swarms, for the construction and disassembly of structures.

The addition of sensors to the flying monkey would also make it a useful surveillance tool. The flying monkey can fly to a destination quickly and then crawl in order quietly maneuver through tight spaces.

Furthermore, since the gripper is not an integral part of the flying monkey's structure, it can be replaced by mechanisms with other functions, such as a mating device that allows it to couple with another robot or to latch onto a wall or branch.

X. DISCUSSION & CONCLUSIONS

While the three capabilities enabled in the flying monkey are sufficient to complete a variety of tasks as listed above, we envision the next generation of such devices to include other abilities, such as cutting / milling / machining, heating / cooling, deposition of glue, etc to facilitate a wider set of applications. Future work must draw from research in swarms as such functionality will only be achieved through the coordination and cooperation between groups of devices with different sets of abilities. The autonomy demonstrated in this paper is the first step to realizing these capabilities. The authors would also like to further this research to increase the mission life of the flying monkey by harnessing the immense potential of the multi-modal transport towards energy efficient trajectories and power optimized path planning for a large swarm of these robots.

APPENDIX

Videos of the experiments are available in the video attachment and at `http://mrsl.grasp.upenn.edu/yashm/ICRA2016.mov`

ACKNOWLEDGMENT

This research was supported by the National Science Foundation (IIS-1138847, EFRI-1240383 and CCF-1138967) and in part by the Army Research Laboratory (W911NF-08-2-0004) and the Wyss Institute for Biologically Inspired Research.

Any opinions, findings, and conclusions or recommendations expressed in this material are those of the authors and do not necessarily reflect the views of the National Science Foundation.

REFERENCES

[1] Alex Kushleyev, Daniel Mellinger, and Vijay Kumar. Towards a swarm of agile micro quadrotors. In *in Robotics: Science and Systems (RSS*, 2012.

[2] M. Turpin, N. Michael, and V. Kumar. Decentralized formation control with variable shapes for aerial robots. In *Robotics and Automation (ICRA), 2012 IEEE International Conference on*, pages 23–30, May 2012.

[3] Michael Rubenstein, Christian Ahler, and Radhika Nagpal. Kilobot: A low cost scalable robot system for collective behaviors. In *2012 IEEE International Conference on Robotics and Automation*, pages 3293–3298. IEEE, May 2012.

[4] J P Whitney, P S Sreetharan, K Y Ma, and R J Wood. Pop-up book mems. *Journal of Micromechanics and Microengineering*, 21(11):115021, 2011.

[5] P S Sreetharan, J P Whitney, M D Strauss, and R J Wood. Monolithic fabrication of millimeter-scale machines. *Journal of Micromechanics and Microengineering*, 22(5):055027, 2012.

[6] Daniel M Aukes, Benjamin Goldberg, Mark R Cutkosky, and Robert J Wood. An analytic framework for developing inherently-manufacturable pop-up laminate devices. *Smart Materials and Structures*, 23(9):094013, September 2014.

[7] Daler Ludovic, Mintchev Stefano, Stefanini Cesare, and Floreano Dario. A bioinspired multi-modal flying and walking robot. *Bioinspiration & Biomimetics*, 10(1):016005, 2015.

[8] A. Kalantari and M. Spenko. Modeling and performance assessment of the hytaq, a hybrid terrestrial/aerial quadrotor. *Robotics, IEEE Transactions on*, 30(5):1278–1285, 2014.

[9] RJ Wood, S Avadhanula, R Sahai, E Steltz, and RS Fearing. Microrobot design using fiber reinforced composites. *Journal of Mechanical Design*, 130(5):052304, 2008.

[10] Daniel M Aukes and Robert J Wood. PopupCAD : a Tool for Automated Design , Fabrication , and Analysis of Laminate Devices . In *SPIE.DSS*, 2015.

[11] C.D. Onal, M.T. Tolley, R.J. Wood, and D. Rus. Origami-inspired printed robots. *Mechatronics, IEEE/ASME Transactions on*, 20(5):2214–2221, Oct 2015.

[12] Cagdas D Onal, Robert J Wood, and Daniela Rus. Towards printable robotics: Origami-inspired planar fabrication of three-dimensional mechanisms. In *Robotics and Automation (ICRA), 2011 IEEE International Conference on*, pages 4608–4613. IEEE, 2011.

[13] Samuel M Felton, Michael T Tolley, ByungHyun Shin, Cagdas D Onal, Erik D Demaine, Daniela Rus, and Robert J Wood. Self-folding with shape memory composites. *Soft Matter*, 9(32):7688–7694, 2013.

[14] Michael T Tolley, Samuel M Felton, Shuhei Miyashita, Daniel Aukes, Daniela Rus, and Robert J Wood. Self-folding origami: shape memory composites activated by uniform heating. *Smart Materials and Structures*, 23(9):094006, 2014.

[15] S Felton, M Tolley, E Demaine, D Rus, and R Wood. A method for building self-folding machines. *Science*, 345(6197):644–646, 2014.

[16] Richard J. Bachmann, Frank J. Boria, Ravi Vaidyanathan, Peter G. Ifju, and Roger D. Quinn. A biologically inspired micro-vehicle capable of aerial and terrestrial locomotion. *Mechanism and Machine Theory*, 44(3):513–526, 2009.

[17] Matthew A. Woodward and Metin Sitti. Multimo-bat: A biologically inspired integrated jumpinggliding robot. *The International Journal of Robotics Research*, 33(12):1511–1529, 2014.

[18] Alexis Lussier Desbiens, Morgan T Pope, David L Christensen, Elliot W Hawkes, and Mark R Cutkosky. Design principles for efficient, repeated jumpgliding. *Bioinspiration and Biomimetics*, 9(2):025009, 2014.

[19] Paul Birkmeyer, Kevin Peterson, and Ronald S Fearing. Dash: A dynamic 16g hexapedal robot. In *Intelligent Robots and Systems, 2009. IROS 2009. IEEE/RSJ International Conference on*, pages 2683–2689. IEEE, 2009.

[20] Daniel M. Aukes and Robert J. Wood. Algorithms for Rapid Development of Inherently-Manufacturable Laminate Devices. In *ASME Conference on Smart Materials, Adaptive Structures and Intelligent Systems*, pages V001T01A005–V001T01A005, Newport, RI, USA, 2014. ASME.

[21] popupCAD. http://www.popupcad.org/.

[22] Y. Mulgaonkar, G. Cross, and V. Kumar. Design of small, safe and robust quadrotor swarms. In *Robotics and Automation (ICRA), 2015 IEEE International Conference on*, pages 2208–2215, May 2015.

[23] Nicola Bezzo, Matthew Piccoli, Peter Gebhard, Vijay Kumar, Mark Yim, and Insup Lee. Rapid co-design of electro-mechanical specifications for robotic systems. In *ASME 2015 International Design Engineering Technical Conferences and Computers and Information in Engineering Conference*. American Society of Mechanical Engineers, August 2015.

[24] Pixhawk. http://www.pixhawk.org/.

[25] Taeyoung Lee, M. Leoky, and N.H. McClamroch. Geometric tracking control of a quadrotor uav on se(3). In *Decision and Control (CDC), 2010 49th IEEE Conference on*, pages 5420–5425, Dec 2010.

[26] Robot Operating System (ROS). http://www.ros.org/.